Nuclear Science and Techniques (2024) 35:45
https://doi.org/10.1007/s41365-024-01398-1

Analyzing the surface passivity effect of germanium oxynitride: a comprehensive approach through first principles simulation and interface state density

Sheng-Jie Du[1] · Xiu-Xia Li[2] · Yang Tian[3] · Yuan-Yuan Liu[1] · Ke Jia[4] · Zhong-Zheng Tang[1] · Jian-Ping Cheng[1] · Zhi Deng[3] · Yu-Lan Li[3] · Zheng-Cao Li[4] · Sha-Sha Lv[1]

Received: 15 May 2023 / Revised: 17 August 2023 / Accepted: 16 September 2023 / Published online: 9 April 2024

Abstract

High-purity germanium (HPGe) detectors, which are used for direct dark matter detection, have the advantages of a low threshold and excellent energy resolution. The surface passivation of HPGe has become crucial for achieving an extremely low energy threshold. In this study, first-principles simulations, passivation film preparation, and metal oxide semiconductor (MOS) capacitor characterization were combined to study surface passivation. Theoretical calculations of the energy band structure of the –H,–OH, and $–NH_2$ passivation groups on the surface of Ge were performed, and the interface state density and potential with five different passivation groups with N/O atomic ratios were accurately analyzed to obtain a stable surface state. Based on the theoretical calculation results, the surface passivation layers of the Ge_2ON_2 film were prepared via magnetron sputtering in accordance with the optimum atomic ratio structure. The microstructure, *C-V*, and *I-V* electrical properties of the layers, and the passivation effect of the $Al/Ge_2ON_2/Ge$ MOS were characterized to test the interface state density. The mean interface state density obtained by the Terman method was 8.4×10^{11} cm^{-2} eV^{-1}. The processing of germanium oxynitrogen passivation films is expected to be used in direct dark matter detection of the HPGe detector surface passivation technology to reduce the detector leakage currents.

Keywords Surface passivation · High purity germanium detector · Germanium nitrogen oxide · Interface state density

1 Introduction

High-purity germanium (HPGe) detectors have the advantages of low background, low energy threshold, and high energy resolution, and are widely used in fields such as nuclear astrophysics [1–3], geography [4], and materials science [5–8]. HPGe detector array systems are very competitive in detecting rare events such as dark matter and $0\nu\beta\beta$ [9, 10]. Many international experimental groups, including the China Dark Matter Experiment [11–15] (CDEX), Coherent Germanium Neutrino Technology (COGENT) [16], EDELWEISS [17], Germanium Detector Array [18] (GERDA), MAJORANA [19], and Super Cryogenic Dark Matter Search [20] (SuperCDMS), have carried out relevant rare event detection experiments with high-purity germanium detectors [21, 22]. Specifically, a low threshold for HPGe detectors is crucial for the sensitivity of dark matter detection. Dark matter theory predicts that lowering the detector energy threshold can not only

---

This work was supported by the National Natural Science Foundation of China (No. 12005017).

✉ Sha-Sha Lv
lvss@bnu.edu.cn

[1] College of Nuclear Science and TechnologyJoint Laboratory of Jinping Ultra-Low Radiation Background Measurement of Ministry of Ecology and EnvironmentKey Laboratory of Beam Technology of Ministry of Education, Beijing Normal University, Beijing Normal University, Beijing 100875, China

[2] Joint Research Center, Nuctech Company Limited, Beijing 100084, China

[3] Department of Engineering Physics, Key Laboratory of Particle & Radiation Imaging of Ministry of Education, Tsinghua University, Beijing 100084, China

[4] Key Laboratory of Advanced Materials (MOE), School of Materials Science and Engineering, Tsinghua University, Beijing 100084, China

reduce the lower mass limit of detectable particles, but also increase the event rate with the exponential law of dark matter interacting with the detector target nucleus. In addition, the theory proposes strict requirements for the background environment, detector sensitivity, and long-term stability.

The interface-state problem in the use of germanium-based devices is puzzling. The band gap of Ge (0.67 eV) is smaller than that of Si (1.12 eV) at room temperature. The hole and electron mobilities of germanium are 4.2 and 2.6 times those of silicon [23, 24], respectively, which results in a large leakage current for the HPGe detector. With many dangling bonds at the surface of the HPGe- and Ge-based devices, the surface leakage current becomes the main influential factor. A new passivation layer is needed to replace silica and thus solve small-size metal oxide semiconductor (MOS) devices and HPGe detectors, which will have higher chemical stability, dielectric constant, and decreased leakage current. Regarding the surface characteristics of germanium oxides, the volatile GeO and soluble in water GeO_2 lead to poor conductivity, interfacial state, and stability of HPGe. GeO_2 on the surface reacts with Ge to generate GeO, which further increases the leakage current [25, 26].

Processes for surface passivation of HPGe include wet chemical processing and sputtering [26–28]. These processes, which should be performed at room temperature to avoid the diffusion of Li^+ and B^+ at high temperatures, further expand the detector dead layer and reduce the sensitive volume. Wet chemical processing typically uses a mixture of H_2O_2, HNO_3, HF, and H_3PO_4 to oxidize the HPGe surface and produces a dense oxide film. Meanwhile, the sputtering film includes silicon oxides, amorphous germanium, and amorphous silicon [27, 29]. The lattice mismatch at the interface between silicon oxide and germanium makes it difficult to guarantee the stability of the HPGe detector. Compared to GeO_2, Ge_3N_4 and GeO_xN_y, which have improved chemical stability, are expected to provide a passivation layer for germanium-based devices with good performance as the introduction of nitrogen atoms will improve the dielectric constant and stability [30].

In this study, the feasibility and effect of germanium nitrogen oxide as a passivation layer for HPGe were investigated. The band structure and density of states (DOS) of –H, –OH, and $–NH_2$ passivated germanium were investigated using first principles. Five different nitrogen–oxygen atomic ratios of GeO_xN_y were constructed to analyze the density of states near the Fermi level. The GeO_xN_y passivation layer was prepared by magnetron sputtering adjusting the atmospheric, power, and pressure parameters to obtain optimum atomic ratios in accordance with the simulation results. Finally, the interface state density of defects (D_{it}) was analyzed to evaluate the feasibility of GeO_xN_y and provide references for future experimental passivation schemes.

2 Calculation and experimental methods

2.1 Optimization parameter settings of germanium

The unit cell structure of germanium is a cubic crystal system, and the space group is Fd-3 M with a side length of 5.65 Å. First-principles calculations were performed using density functional theory (DFT) with CASTEP in Materials Studio. The generalized gradient approximation (GGA) was employed as an independent exchange–correlation function with a noncanonical conservation pseudopotential (nom conservation). For structural optimization, the k point was $4 \times 4 \times 4$, the truncation energy was 400 eV, and the energy convergence accuracy was 1.0×10^6 eV/atom [29, 31, 32].

The side length of the germanium cell is relaxed to 5.59 Å after geometry optimization. The valence band maximum (VBM) and conduction band minimum (CBM) are located at the γ point and R point with indirect band gap semiconductors. The bandgap width is 0.661 eV, which is similar to the 0.67 eV of the theoretical data [23].

2.2 Passivation model of different termination groups

The Ge cell structure is derived from a diamond structure. The optimized Ge supercell was expanded in the (100) direction and cut off to avoid the influence of periodicity. A vacuum layer of 10 Å was added to the cell with a supercell side length ($d + 10$ Å) in the a-axis direction with nine germanium atoms. The passivation groups were attached to the Ge atoms with broken bonds. The atoms with a vacant outermost electron structure were connected to –H atoms, and 12 passivation atoms or groups formed bonds with the germanium atoms. Two types of germanium atoms have dangling bonds: the first one is in the middle and forms a bond with one atom or group; it is named Ge1. The second type is in the corner and bonds with two atoms or groups; it is named Ge2. After the passivation model structure was established, GGA was selected as the independent exchange–correlation function with no conservation. The k point was $4 \times 1 \times 1$, the truncation energy was 650 eV, and the energy convergence accuracy was 1.0×10^5 eV/atom [29, 32].

2.3 Passivation film preparation and MOS device characterization

A P type germanium substrate with a $< 100 >$crystal orientation was selected, and its resistance was approximately 5–40 Ω. First, the substrate was rinsed with an ultrasonic cleaner consisting of ethanol, acetone, and deionized water for 15 min. A cylindrical magnetron sputtering source was connected to an RF power generator using a matcher. Before film deposition, the pressure of the vacuum chamber was pumped below 3.0×10^{-4} Pa.

Physical characterization of the thin GeO_xN_y passivation layer was performed using electrical characteristics, scanning electron microscopy (SEM), and X-ray photoelectron spectroscopy (XPS). The electrical characteristics and surface-state density of the GeO_xN_y passivation layer were measured using a Keithley 4200A-SCS instrument at room temperature. SEM was performed using a Zeiss Merlin Compact Field Emission Scanning Electron microscope to analysis the passivation layer thickness and uniformity. XPS was performed utilizing a Thermo 250XI with monochromatic X-ray using the Al Kα line.

3 Results and discussion

3.1 Band structure and density of states of Ge passivation (–H, –OH, $–NH_2$)

The ball-and-stick models of Ge with –H, –OH, and $–NH_2$ group passivation are shown in Fig. 1a, b, and c, respectively. The energy location of 0 eV in the figures of band structure and DOS represents the position of the Fermi level. The band gaps of Ge–H, Ge–OH, and $Ge–NH_2$ are 4.06, 2.20, and 1.87 eV, respectively. The Ge–H structure has a direct band gap, whereas the Ge–OH and $Ge–NH_2$ structures have both indirect band gaps. The band structure and DOS of the different atoms or groups were analyzed to determine the rationality of the passivation. The low surface leakage current was confirmed by the moderate bandgap and low D_{it} near the Fermi level.

To understand whether the interface state density was influenced by the different passivation atoms or groups, the total density of states (TDOS) and partial density of states (PDOS) of the passivation system were analyzed. The DOS was analyzed to identify the passivation atoms or group

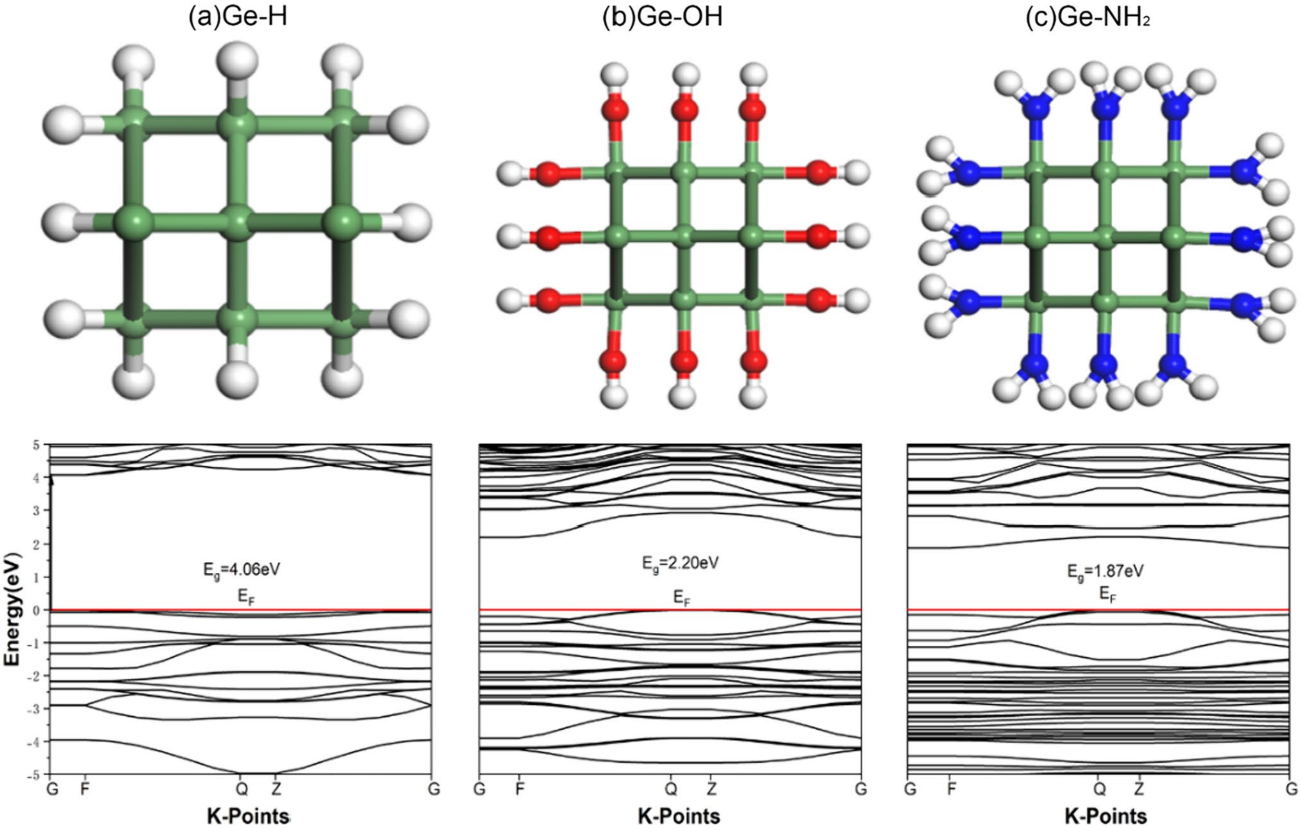

Fig. 1 (Color online) Ball-and-stick models and the corresponding band structures of **a** –H, **b** –OH, and **c** $–NH_2$ termination groups, represented by H atoms (white balls), O atoms (red balls), and N atoms (blue balls), respectively

interactions with the Ge atoms. The atomic interactions and chemical bonds were explored to analyze the DOS. Figure 2a shows the TDOS with the Ge–H, Ge–OH, and Ge–NH_2 terminations. The TDOS of the Ge–OH group near the Fermi level is the smallest, whereas that of the Ge–H group is the largest. Figure 2b, c, and d show the PDOS of Ge–H, Ge–OH, and Ge–NH_2, respectively. As shown in Fig. 2b, the DOS near the VBM is mainly contributed by the 4 *p* orbital of the Ge atom, and the contributions of Ge1 and Ge2 are similar. The DOS near the CBM is mainly contributed by the 4 *s* and 4 *p* orbitals of the Ge atom, and the contribution of the 4 *p* orbital is slightly greater than that of the 4 *s* orbital. As shown in Fig. 2c and d, the DOS near the VBM is mainly contributed by the 2 *p* orbital of the O and N atoms, which is related to the electronegativity of these atoms being greater than that of the H atoms. The Ge2 atoms in the Ge–OH and Ge–NH_2 structures are shifted to the left in the valence band compared to those in the Ge–H structure. In the structure of the Ge–OH passivation, the 2 *p* orbital of the O atom has more interactions with the 4 *p* orbital of the Ge atom. For the Ge–NH_2 passivation system, the 4 *p* orbital of Ge1 interacts more with the 2 *p* orbital of N, and the 4 *s* orbital of Ge2 interacts more with the Ge1 atom. Among the three systems, the –OH passivation group with a moderate bandgap width and small DOS should be selected.

3.2 Band structure of Ge–O_xN_y passivation

With the exception of Ge–O_2N_2, which has a direct bandgap with the VBM and CBM located at the K-point of γ, the other passivation structures show indirect bandgap characteristics. The VBM of Ge–O_2N and Ge–ON_2 are located at the Q–Z point in the K space. The VBM of Ge–ON and Ge–O_3N are located at the γ point. The CBM of Ge–ON and Ge–O_3N are located at the γ point, whereas the CBM of Ge–O_2N and Ge–ON_2 are located at the F and Q–Z points.

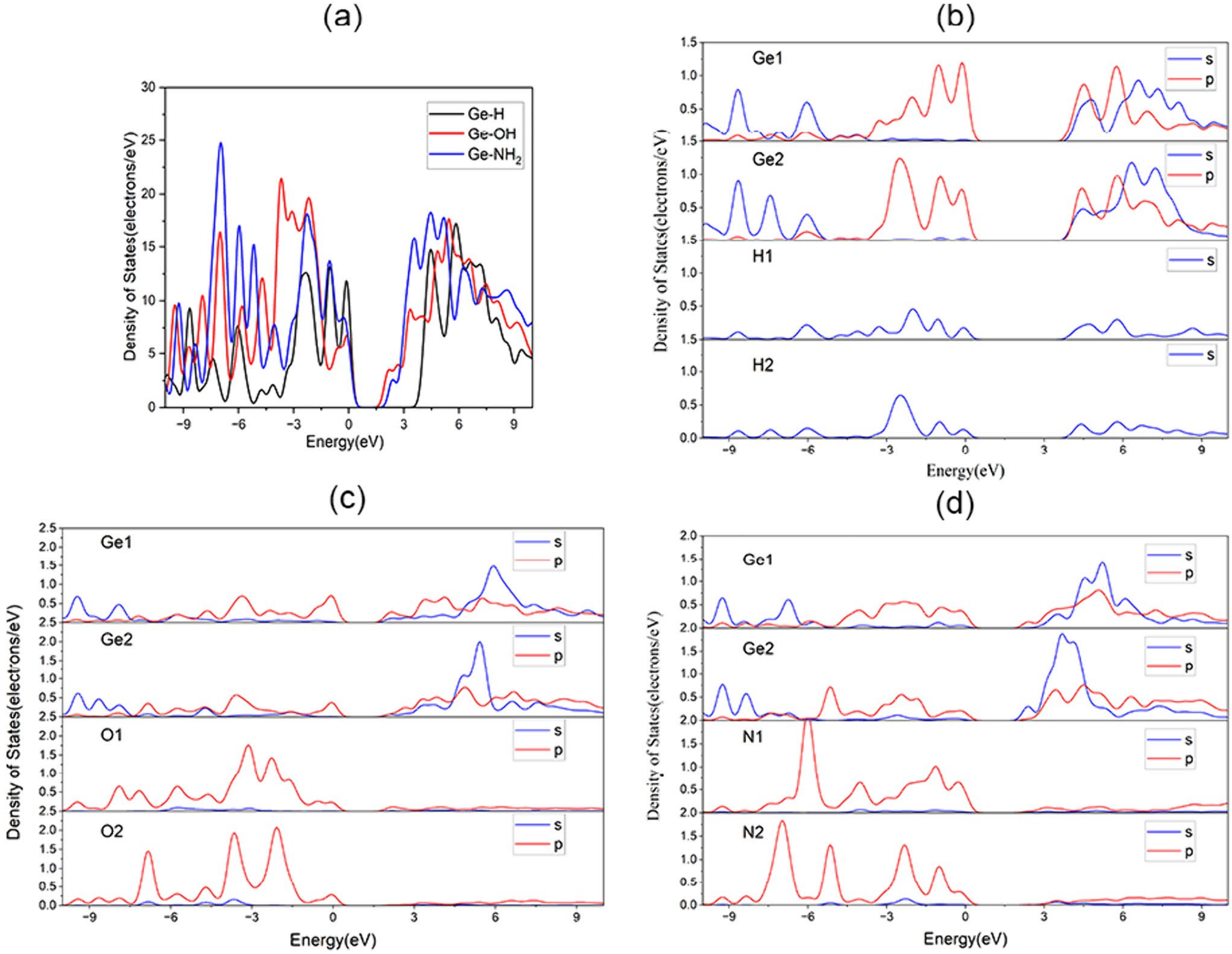

Fig. 2 (Color online) **a** –H, –OH, and –NH_2 terminations of the total density of states (TDOS), and partial density of states (PDOS) of the **b** –H, **c** –OH, and **d** –NH_2 terminations

The bandgap widths of –ON, –O_2N, –O_3N, –ON_2, and –O_2N_2 are 1.81, 0.919, 0.615, 1.568, and 1.124 eV, respectively. The VBM of Ge–ON and Ge–ON_3 are located at the Q–Z point in the K space. The CBM and VBM of Ge–O_2N are located at the F and γ points, and the VBM and CBM of –ON_2 are located at γ and Q–Z points. The increase in the number of either O or N atoms can affect the bandgap width, which may lead to the generation of other energy levels, and the O atom has a greater role in reducing the bandgap width (Fig. 3).

3.3 DOS of Ge–O_xN_y passivation

The DOS is influenced by different nitride and oxygen atom ratios, which were researched by analyzing the DOS of the five systems. Figure 4 shows the TDOS diagrams of the five passivation groups with different N/O ratios. The highest TDOS near the Fermi level is for Ge-ON, whereas the lowest TDOS near the Fermi level is for Ge–O_3N. To further analyze the optimal N/O atomic ratios of the passivation groups in the PDOS diagram, the Ge atoms in the different passivation environments were named Ge1 and Ge2 based on the previous definition. The other passivated atoms were named A*X*-B (where A represents the passivated atom, *X* indicates the number of passivation atoms, and B denotes the directly connected atom).

The two Ge PDOS conditions are shown in Fig. 5. Overall, the contributions of the 4 *s* and 4 *p* orbitals in the vicinity of the VBM (– 5–0 eV) are very weak for both Ge1 and Ge2 atoms. The contribution of the 4 *p* orbital is slightly larger than that of the 4 *s* orbital. Both the Ge1 and Ge2 atoms contribute more to the PDOS in the CBM. The contributions of 4 *s* and 4 *p* orbitals near the vicinity of the CBM are equivalent, with the exception of Ge-O_3N. For the PDOS of Ge1 atoms, the introduction of O atoms causes a DOS in the left direction, and the same situation occurs for the PDOS of Ge2 atoms. N atoms also cause a PDOS shift toward the left for Ge1 atoms, but this is not obvious for Ge2 atoms. This finding indicates that N atoms have a large influence on less-bonded Ge atoms, and that O atoms have the same influence on unbonded Ge atoms.

Different O/N ratios have distinct effects on the DOS of these systems. The effects of O and N atoms on the DOS warrant further study. Figure 6 shows the PDOS diagrams of the O atoms in different environments. The O atoms significantly contribute to the DOS of the valence band, which is provided by the 2 *p* orbital. When a Ge2 atom is passivated by an O atom, the DOS in the valence band shifts to the left as the number of O atoms increases. Combined with the previous analysis for Ge atoms, O atoms cause the entire DOS to move toward the left. As shown in the PDOS diagram of the N atom in Fig. 7, N atoms directly connected to Ge atoms contribute slightly to the conduction band, with the exception of Ge–O_2N_2 passivation. The DOS near the VBM of the N atoms connected to the Ge atoms is almost unaffected by the number of O or N atoms in the systems. The N atoms that are connected to the O atoms in the Ge–O_2N_2 system have an effect similar to that of the Ge atoms. However, we discovered that such an anomaly appeared in the structure of O_2N_2. We speculate that the electronegativity of

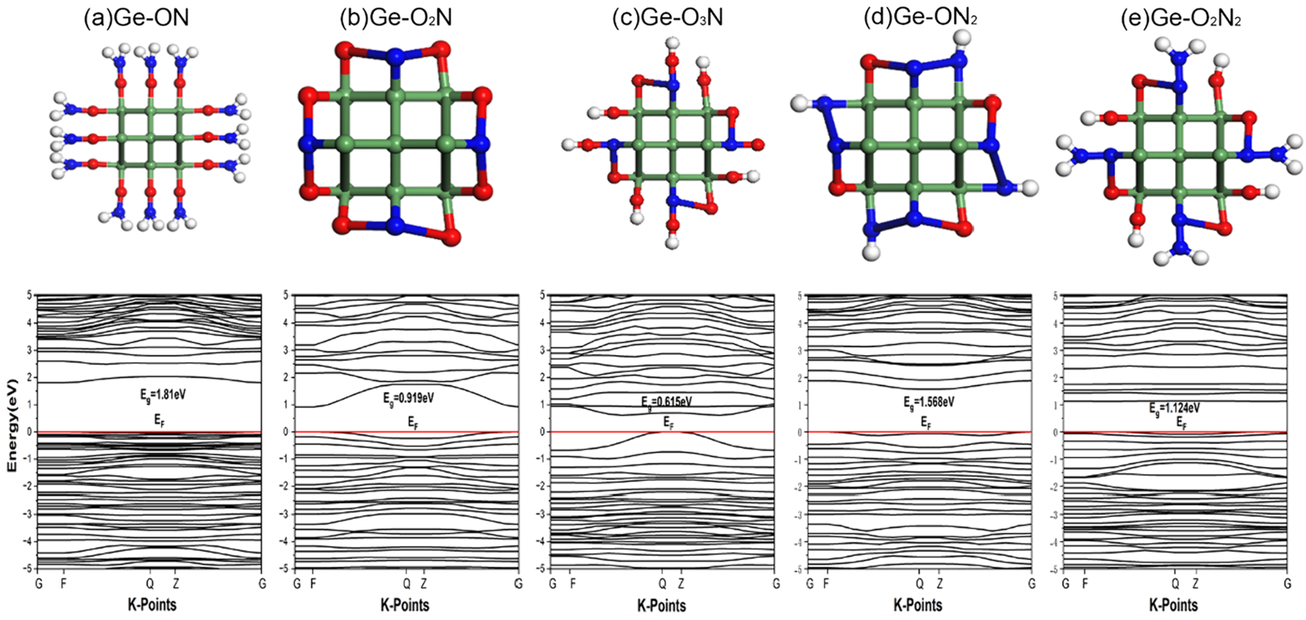

Fig. 3 (Color online) Ball-and-stick models and the corresponding band structures of **a** Ge–ON, **b** Ge–O_2N, **c** Ge–O_3N, **d** Ge ON_2, and **e** Ge–O_2N_2 termination groups

Fig. 4 (Color online) TDOS of nitrogen oxides of germanium

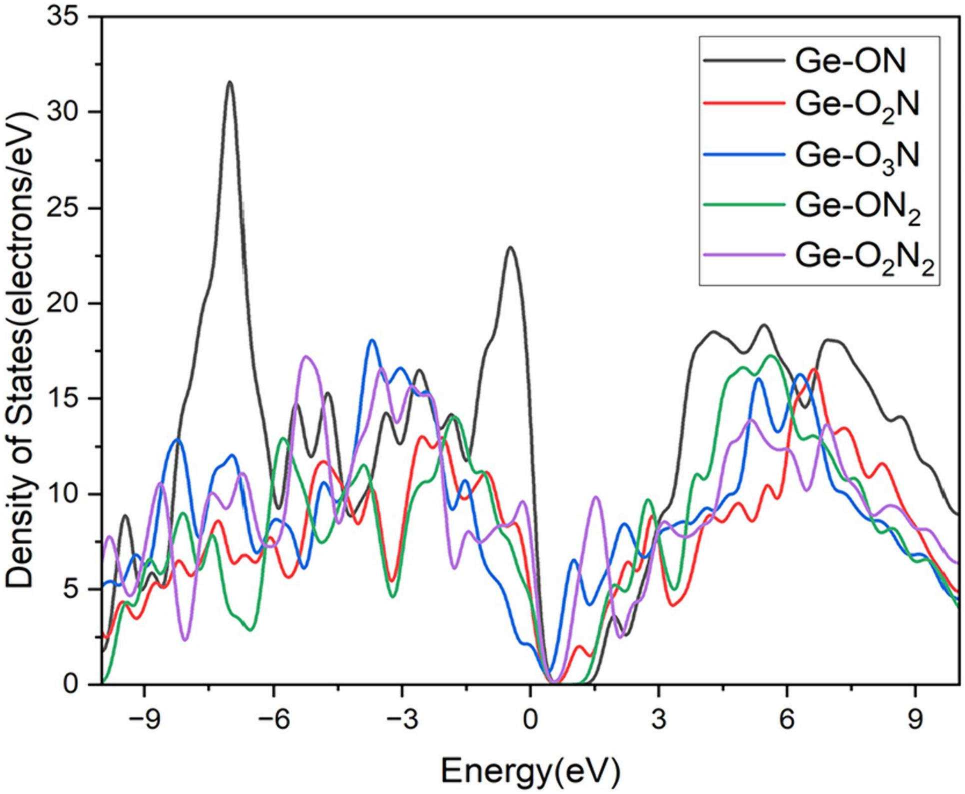

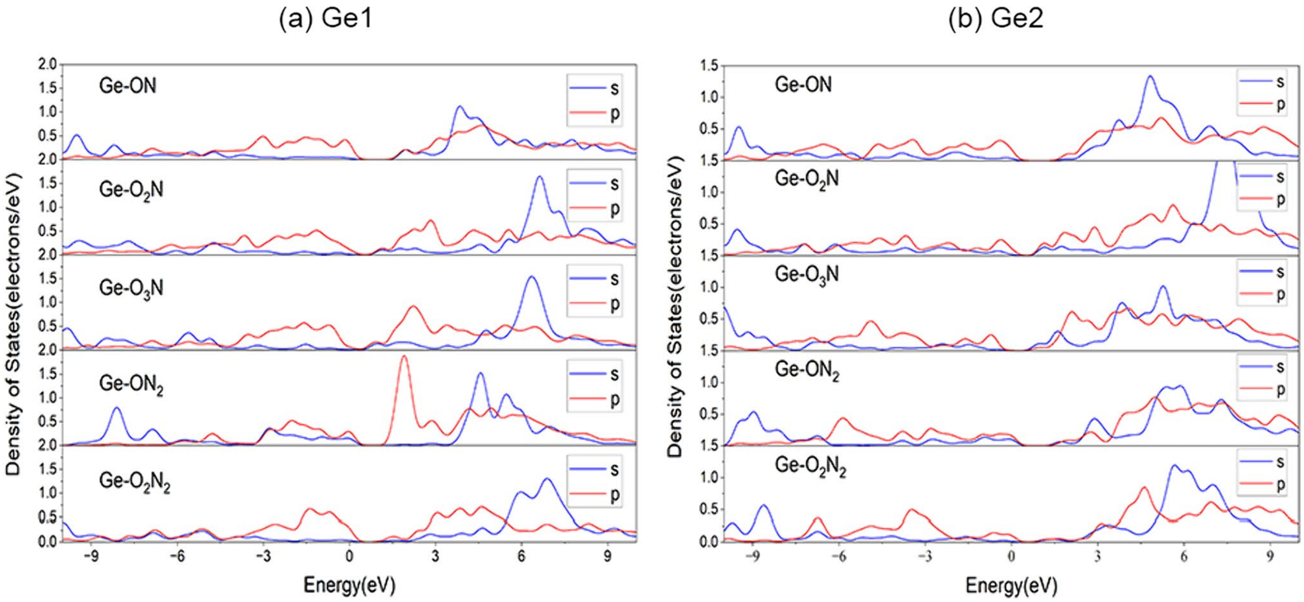

Fig. 5 (Color online) PDOS of nitrogen oxides of germanium: **a** Ge1 PDOS and **b** Ge2 PDOS

the N atom is strong, and the adjacent N–Ge bond is weak when the N–N bond is formed.

When connected to the Ge1 atom, an increase in the number of N atoms causes the DOS to shift to the left. However, the DOS of the O atoms directly connected to the N atoms is very small, indicating that the 2 *p* orbital of the O atoms does not interact strongly with the 2 *p* orbital of N (N–O_3N). The same result occurs in Ge–ON, where the Ge atom is directly passivated by the O atom, showing the similarity of this structure to –OH passivation. Instead, the

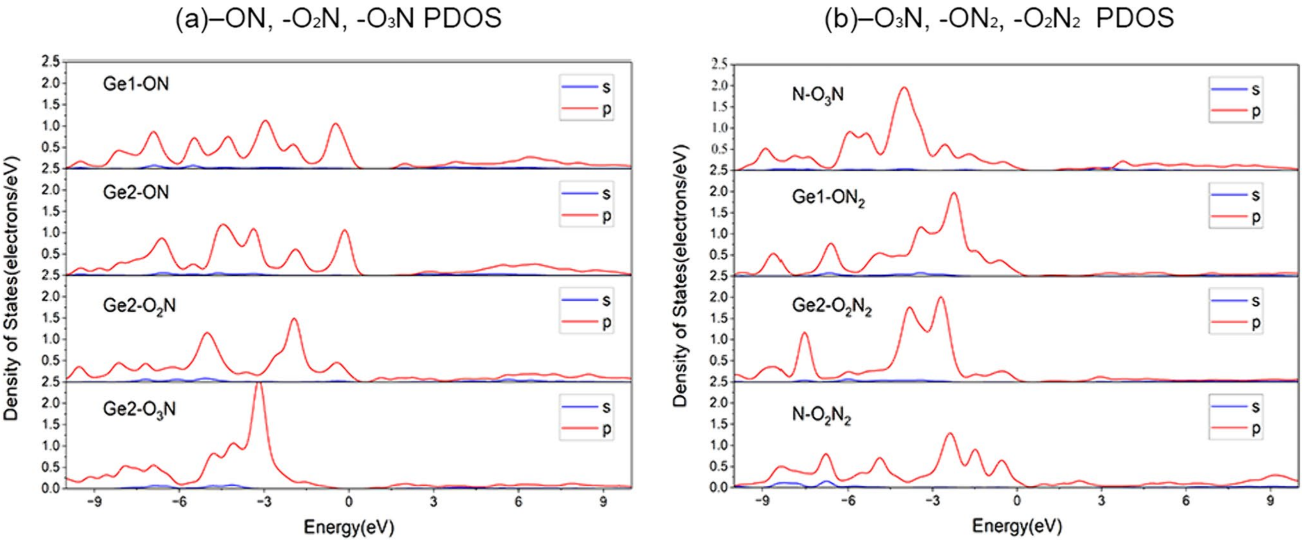

Fig. 6 (Color online) O PDOS of nitrogen oxides of germanium: **a** –ON, –O_2N, –O_3N, and **b** –O_3N, –O_2N, –O_2N_2

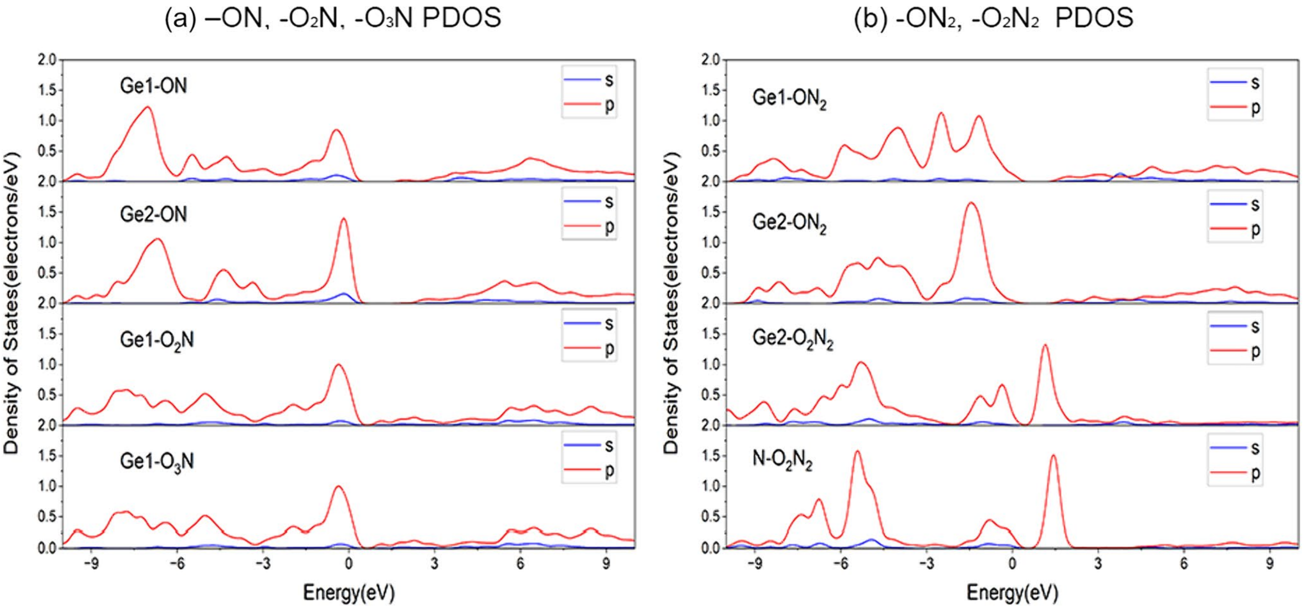

Fig. 7 (Color online) N PDOS of nitrogen oxides of germanium: **a** –ON, –O_2N, –O_3N, and **b** –ON_2, –O_2N_2

O and N atoms passivated the Ge as a whole. Although the Ge–O_3N structure has the lowest DOS, its band gap width is only 0.615 eV, near the 0.67 eV of Ge itself. Therefore, the best passivation effect of the Ge–ON_2 group is obtained with a gap width of 1.568 eV, and its DOS is similar to that of Ge–O_3N.

For the germanium passivation calculation, Houssa et al. determined that there are few defects at the Ge/GeO_2 interface using first principles [33]. Under ideal conditions, the interfacial state density is only 10^{11} cm^{-2} eV^{-1}, which is even lower than the detection limit of electron spin resonance (ESR). Saito et al. calculated that the Ge/GeO_2 interface is more flexible than the Si/SiO_2 interface [34]. Atomic Ge emissions can be inhibited during the oxidation process to change the electrical properties of the Ge/GeO_2 interface. The germanium detector was passivated by applying appropriate oxygen–nitrogen ratios to reduce the interface state density and surface leakage current. Based on the number of Ge and passivation atoms obtained from our calculations, the optimal chemical dose ratio for surface passivation is Ge_2ON_2.

3.4 Interface state density at –O_xN_y passivation

All passivation layers were prepared in a 2:1 nitrogen–oxygen mixed atmosphere on a < 100 > germanium single crystal. The RF power was chosen to be 60–80 W. The prepared oxygen–nitrogen passivation layer film was amorphous and crystalline, with a mixture of various germanium–nitrogen oxides. Figure 8a, b, and c show the XPS spectra of the Ge 3 *d*, N 1 *s*, and O 1 *s* energy levels, respectively. The ratio of the peak area to the sensitivity factor was calculated, which showed that the Ge:N:O atomic ratio of the passivation film was close to 2:1:2 [35]. The peak values corresponding to the binding energy of GeO_2, GeON, and Ge_3N_4 were 33.2, 32.2, and 32.1 eV [36, 37], respectively.

To extract information regarding the interface state density, the *I-V* and *C-V* characteristics of the Al/Ge_2ON_2/Ge MOS structure passivated with germanium nitrogen oxides at room temperature are shown in Fig. 8d and e. A higher D_{it} affected the passivation results for a low leakage current and threshold. The IV characteristics in the scanning range of − 1.5–1.5 V and the capacitance characteristics from − 1 to 1 V of the GeO_xN_y passivation layer with a thickness of 20 nm are analyzed.

It is difficult to determine the dielectric constant of a passivated film owing to its amorphous state, which makes it difficult to determine the capacitance of the oxide layer. In the $\frac{1}{c}\left(\mathrm{pF}^{-1}\right)$ vs. $\sqrt{\frac{\mathrm{d}}{\mathrm{d}V_{\mathrm{G}}}\frac{1}{c^2}}\left(\mathrm{V}^{-\frac{1}{2}}\mathrm{pF}^{-1}\right)$ curves shown in Fig. 9a, the *x*-intercept of the fitted curve could be recognized as an oxide layer capacitance of 8.9×10^{-9} F. The D_{it} calculation using the Terman method is shown in Eq. (1) [38, 39]:

$$D_{\mathrm{it}} = \frac{C_{\mathrm{OX}}}{q^2}\left(\frac{\mathrm{d}V_{\mathrm{G}}}{\mathrm{d}\varphi_{\mathrm{s}}} - 1\right) - \frac{C_{\mathrm{s}}}{q^2} = \frac{C_{\mathrm{OX}}}{q^2}\frac{\mathrm{d}\Delta V_{\mathrm{G}}}{\mathrm{d}\varphi_{\mathrm{s}}} \tag{1}$$

where C_{OX} and C_{s} are the oxide layer and semiconductor capacitance, respectively, q is the electron charge size (1.6×10^{-19} C), ΔV_{G} represents the difference between the *C-V* characteristics measured in the experiment and ideal curve, and φ_{s} represents the surface potential. The Terman method has many approximations and the calculation of the doping concentration and oxidation capacitance leads to an overestimation of D_{it} [40]. The distribution of D_{it} with the energy levels is given by Eq. (2) [41]:

$$E_{\mathrm{c}} - E_{\mathrm{T}} = q\varphi_{\mathrm{s}} + \left(E_{\mathrm{c}} - E_{\mathrm{F}}\right) \tag{2}$$

where E_{c} is the conduction band of the semiconductor, E_{F} is the Fermi level, and E_{T} is the trap energy at the interface. The interface energy level distribution near the band

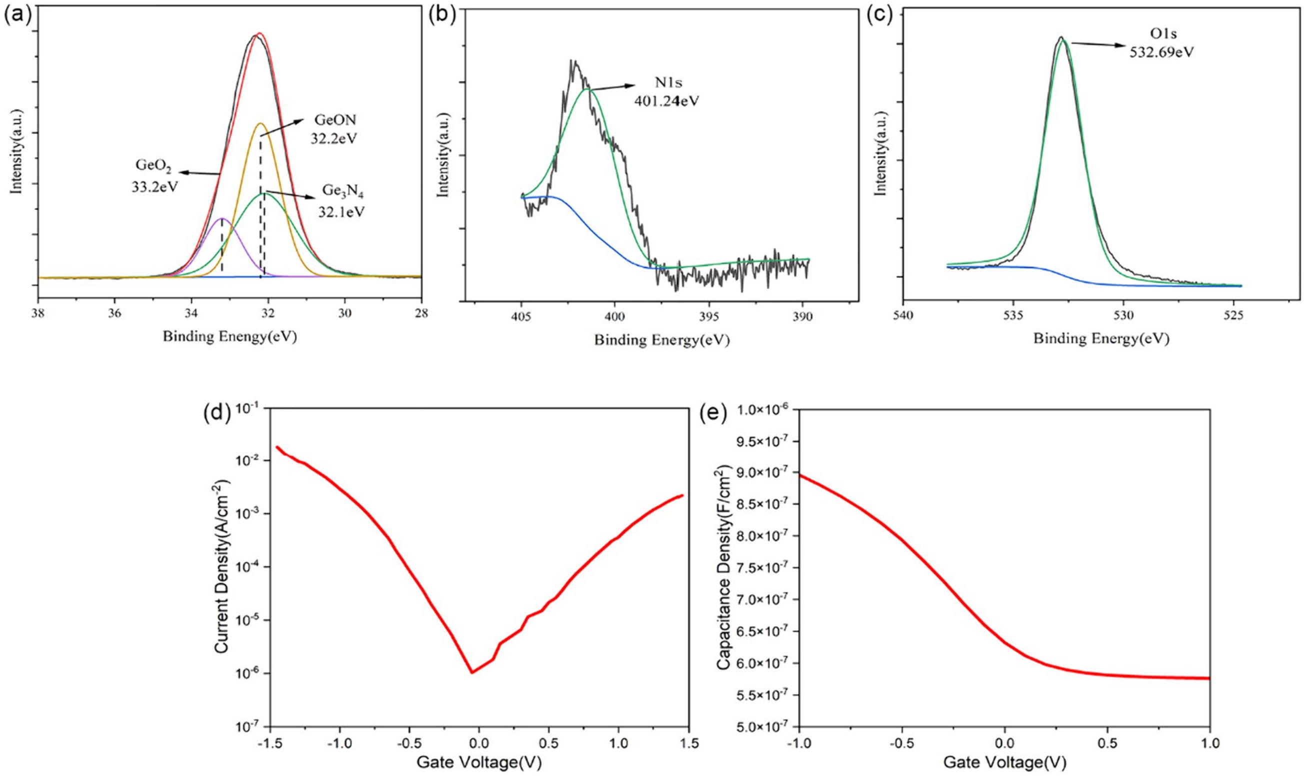

Fig. 8 (Color online) Al/Ge_2ON_2/Ge MOS structural characteristics: XPS spectra of the **a** Ge 3 *d*, **b** N 1 *s*, and **c** O 1 *s* energy levels of the Ge_2ON_2 film; **d** *I-V* characteristic, and **e** *C-V* characteristic

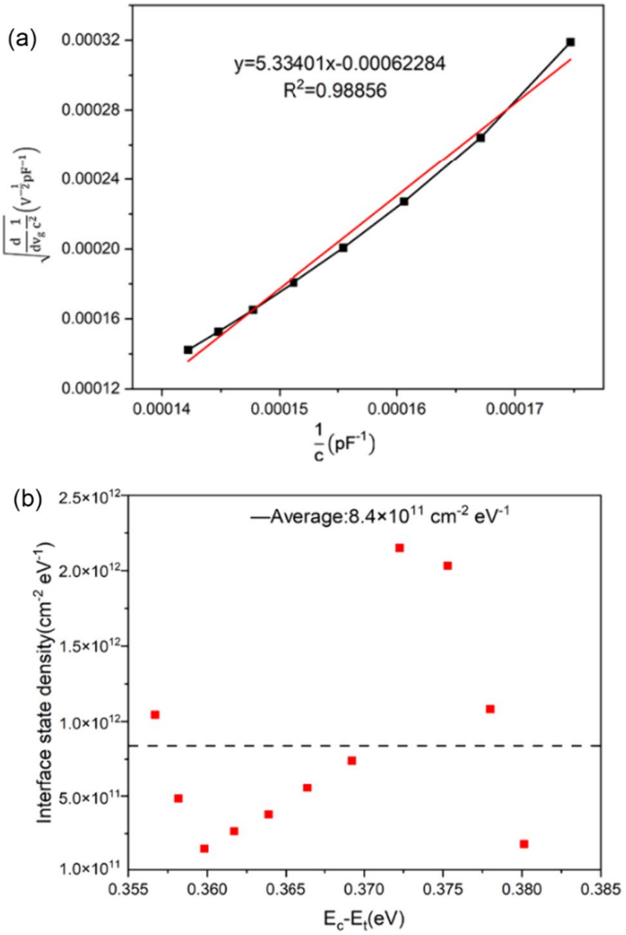

Fig. 9 **a** Cox fitting curve and **b** density of interfacial states at different energy level positions

energy level (E_c) ranges approximately from $E_c - 0.29$ to $E_c - 0.31$ eV.

Figure 9b shows an average interface state density of 8.4×10^{11} cm^{-2} eV^{-1}, which indicates that it is feasible to passivate the HPGe detector by magnetron sputtering GeO_xN_y at room temperature for a lower D_{it}. D_{it} is uniformly distributed at this energy level, indicating that the amorphous states do not have obvious interface defects. The low surface defects are confirmed by the low D_{it}, and the low surface leakage current is caused by the low defects at the Ge_2ON_2/Ge interface. In addition, some abnormal D_{it} values deviate significantly from the average, which is attributed to the presence of amorphous GeO_xN_y at the interface. This finding is consistent with previous simulation results: as the number of nitrogen and oxygen atoms increases, more dangling bonds of germanium are formed, and the interface state density is further reduced. Germanium nitrogen oxide passivation of the reported HPGe detector achieved low leakage (~ pA) and good performance [30, 42, 43]. The interface state density and leakage current at low temperatures should be investigated in future studies.

4 Conclusion

Based on first principles, passivation groups of Ge–H, Ge–OH, and Ge–NH_2 structures were simulated to analyze the band structure and DOS of Ge passivation. Ge–OH was found as the best passivation group. Furthermore, the introduction of N atoms improved the stability of the Ge passivation layer. Five different N/O ratios of Ge–ON, Ge–O_2N, Ge–O_3N, Ge–ON_2, and Ge–O_2N_2 were used to analyze the feasibility of HPGe passivation by Ge oxynitride using first principles. N and O atoms lead to a reduction in the bandgap width, and the passivation atoms directly connected to the Ge atoms have a more significant effect. The 4 *p* orbitals of Ge in the conduction band and 2 *p* orbitals of O and N in the valence band interact to affect the DOS in most systems. Considering the influence of the bandgap width and DOS, a passivation group with a moderate bandgap width and small interfacial state density should be selected. A higher interface state density may affect the passivation results of low leakage current and threshold for the HPGe detector. Therefore, Ge-ON_2 with a bandgap width of 1.568 eV and a relatively low DOS, which is only slightly higher than that of Ge–O_3N, is the best choice.

The low interfacial state density plays a crucial role in ensuring low leakage in the HPGe detector. To further verify our simulation, a germanium nitrogen oxide passivation film was prepared by magnetron RF sputtering of a germanium single crystal to obtain a Ge/O/N atomic ratio of 2:1:2. The *I-V* and *C-V* characteristics of the Al/Ge_2ON_2/Ge MOS capacitors were measured at room temperature. The interface state density near the valence band was calculated by the Terman method, and the average density was 8.4×10^{11} cm^{-2} eV^{-1}. The low number of surface defects between the Ge_2ON_2/Ge surfaces was confirmed by the low D_{it}. The results of capacitance and D_{it} indicate that germanium oxynitride can be used as a new passivation layer to replace silicon oxide and further reduce the leakage current and provide long-term stability. Further detailed tests will be conducted to determine the best performance of the passivated layer film-like test at liquid nitrogen temperature and to achieve the requirements of the next experimental program for direct detection of rare events using the HPGe detector.

Acknowledgements The authors thank the Key Laboratory of Particle Technology and Radiation Imaging (Ministry of Education) at the Tsinghua University, which is a member of the China Dark Matter Experimental Cooperation Group.

Author contributions SJD, XXL, YT, JPC and SSL contributed to the overall research concept and supervision of this study. SJD, XXL, KJ, ZZT, ZD, and SSL participated in material preparation, data collection, data processing program writing, and data analysis. YYL, YLL, ZCL, and SSL provided experimental suggestions and optimized experimental condition. The first draft of the manuscript was written by SJD, and all authors commented on previous versions of the manuscript. All authors read approved final manuscript.

Data availability The data that support the findings of this study are openly available in Science Data Bank at https://cstr.cn/31253.11.sciencedb.14917 and https://doi.org/10.57760/sciencedb.14917.

Declarations

Conflict of interest The authors declare that they have no competing interests.

References

1. A. Boeltzig, A. Best, G. Imbriani et al., Improved background suppression for radiative capture reactions at LUNA with HPGe and BGO detectors. J. Phys. G Nucl. Part Phys. **45**, 025203 (2018). https://doi.org/10.1088/1361-6471/aaa163
2. Y.L. Dang, F.L. Liu, G.Y. Fu et al., New measurement of thick target yield for narrow resonance at Ex = 9.17 MeV in the 13C(p, γ)14N reaction. Chin. Phys. B **28**, 060706 (2019). https://doi.org/10.1088/1674-1056/28/6/060706
3. D.M. Mei, Z.B. Yin, S.R. Elliott, Cosmogenic production as a background in searching for rare physics processes. Astropart. Phys. **31**, 417–420 (2009). https://doi.org/10.1016/j.astropartphys.2009.04.004
4. A. Déjeant, L. Bourva, R. Sia et al., Field analyses of ^{238}U and ^{226}Ra in two uranium mill tailings piles from Niger using portable HPGe detector. J. Environ. Radioact. **137**, 105–112 (2014). https://doi.org/10.1016/j.jenvrad.2014.06.012
5. M.U. Khandaker, P.J. Jojo, H.A. Kassim et al., Radiometric analysis of construction materials using HPGe gamma-ray spectrometry. Radiat. Prot. Dosim. **152**, 33–37 (2012). https://doi.org/10.1093/rpd/ncs145
6. G. Xhixha, M. Alberi, M. Baldoncini et al., Calibration of HPGe detectors using certified reference materials of natural origin. J. Radioanal. Nucl. Chem. **307**, 1507–1517 (2016). https://doi.org/10.1007/s10967-015-4360-6
7. F. Tuo, C.H. Xu, J. Zhang et al., Radioactivity analysis following the Fukushima Dai-ichi nuclear accident. Appl. Radiat. Isot. **78**, 77–81 (2013). https://doi.org/10.1016/j.apradiso.2013.04.002
8. S. Feng, R. Liu, X.X. Lu et al., A study of ^{239}Pu production rate in a water cooled natural uranium blanket mock-up of a fusion-fission hybrid reactor. Nucl. Fusion **56**, 036019 (2016). https://doi.org/10.1088/0029-5515/56/3/036019
9. J. Zhu, H. Li, T. Xue et al., Prototype of pulse digitizer and readout electronics for CDEX-10 in CJPL. J. Inst. **15**, T01002 (2020). https://doi.org/10.1088/1748-0221/15/01/T01002
10. Z.Y. Zhang, L.T. Yang, Q. Yue et al., Constraints on Sub-GeV Dark Matter-Electron Scattering from the CDEX-10 Experiment. Phys. Rev. Lett. **129**, 221301 (2022). https://doi.org/10.1103/PhysRevLett.129.221301
11. Z. Liu, Q. Yue, L. Yang et al., Constraints on spin-independent nucleus scattering with sub-GeV weakly interacting massive particle dark matter from the CDEX-1B experiment at the China Jinping underground laboratory. Phys. Rev. Lett. **123**, 161301 (2019). https://doi.org/10.1103/PhysRevLett.123.161301
12. Z.F. Lu, Y.L. Li, J. Li et al., MSE/SSE discrimination methods of the PC-HPGe detector. Chin. Phys. C **36**, 855–860 (2012). https://doi.org/10.1088/1674-1137/36/9/011
13. Y.Y. Liu, J.P. Cheng, P. Pang et al., Developing cold-resistant high-adhesive electronic substrate for WIMPs detectors at CDEX. Chin. Phys. B **29**, 045203 (2020). https://doi.org/10.1088/1674-1056/ab718a
14. L. Zhang, C.K. Qiao, J.J. Zhu et al., Preparation of large volume solid argon crystal and its feasibility test as a scintillation material. Crystals **12**, 1416 (2022). https://doi.org/10.3390/cryst12101416
15. Y. Wang, Z. Zeng, Q. Yue et al., First experimental constraints on WIMP couplings in the effective field theory framework from CDEX. Sci. China Phys. Mech. **64**, 281011 (2021). https://doi.org/10.1007/s11433-020-1666-8
16. C.E. Aalseth, P.S. Barbeau, N.S. Bowden et al., Results from a search for light-mass dark matter with a p-type point contact germanium detector. Phys. Rev. Lett. **106**, 131301 (2011). https://doi.org/10.1103/PhysRevLett.106.131301
17. E. Armengaud, C. Augier, A. Benoît et al., Searching for low-mass dark matter particles with a massive Ge bolometer operated above ground. Phys. Rev. D **99**, 082003 (2019). https://doi.org/10.1103/PhysRevD.99.082003
18. M. Agostini, G. Araujo, A. Bakalyarov et al., Final results of GERDA on the search for neutrinoless double-β decay. Phys. Rev. Lett. **125**, 252502 (2020). https://doi.org/10.1103/PhysRevLett.125.252502
19. C.E. Aalseth, N. Abgrall, E. Aguayo et al., Search for neutrinoless double-β decay in Ge-76 with the majorana demonstrator. Phys. Rev. Lett. **120**, 132502 (2018). https://doi.org/10.1103/PhysRevLett.120.132502
20. R. Agnese, T. Aramaki, I.J. Arnquist et al., Results from the super cryogenic dark matter search experiment at Soudan. Phys. Rev. Lett. **120**, 061802 (2018). https://doi.org/10.1103/PhysRevLett.120.061802
21. G. Gelmini, P. Gondolo, DM production mechanisms. arXiv preprint arXiv:1009.3690 (2010)
22. M. Balata, N. Marco, M. Junker et al., Characterization of inverted coaxial 76 Ge detectors in GERDA for future double-β decay experiments. Eur. Phys. J. C **81**, 505 (2021). https://doi.org/10.1140/epjc/s10052-021-09184-8
23. J. Eberth, J. Simpson, From Ge (Li) detectors to gamma-ray tracking arrays–50 years of gamma spectroscopy with germanium detectors. Prog. Part. Nucl. Phys. **60**, 283–337 (2008). https://doi.org/10.1016/j.ppnp.2007.09.001
24. S.M. Sze, *Semiconductor devices: physics and technology*, 3rd edn. (Wiley, New York, 2008), pp.174–176
25. L.P. Etcheverry, H.I. Boudinov, G. Vieira Soares et al., Combining GeO$_2$ passivation strategies aiming at dielectric layers with superior properties on germanium substrates. J. Mater. Chem. C **7**, 8465–8470 (2019). https://doi.org/10.1039/c9tc01831j
26. S. Carturan, G. Maggioni, S.J. Rezvani et al., Wet chemical treatments of high purity Ge crystals for γ-ray detectors: surface structure, passivation capabilities and air stability. Mater. Chem. Phys. **161**, 116–122 (2015). https://doi.org/10.1016/j.matchemphys.2015.05.022
27. M. Amman, Optimization of amorphous Germanium electrical contacts and surface coatings on high purity Germanium radiation detectors. arXiv:1809.03046 (2018)
28. S. Rivillon, Y.J. Chabal, F. Amy et al., Hydrogen passivation of germanium (100) surface using wet chemical preparation. Appl. Phys. Lett. **87**, 253101 (2005)
29. S.S. Lv, Y.Y. Liu, W.Y. Tang et al., Evaluation of the passivation effect and the first-principles calculation on surface termination of germanium detector. Nucl. Sci. Tech. **32**, 93 (2021). https://doi.org/10.1007/s41365-021-00930-x

30. T. Maeda, T. Yasuda, M. Nishizawa et al., Pure germanium nitride formation by atomic nitrogen radicals for application to Ge metal-insulator-semiconductor structures. J. Appl. Phys. **100**, 014101 (2006). https://doi.org/10.1063/1.2206395
31. M.D. Segall, P.J.D. Lindan, M.J. Probert et al., First-principles simulation: ideas, illustrations and the CASTEP code. J. Phys. Condens. Matter **14**, 2717 (2002). https://doi.org/10.1088/0953-8984/14/11/301
32. C.N. He, L. Xu, W.Q. Huang et al., Origin of photocatalytic activity of nitrogen-doped germanium dioxide under visible light from first principles. Mater. Sci. Semicond. Process. **31**, 517–524 (2015). https://doi.org/10.1016/j.mssp.2014.12.035
33. M. Houssa, G. Pourtois, M. Caymax et al., Ge dangling bonds at the (100)Ge/GeO_2 interface and the viscoelastic properties of GeO_2. Appl. Phys. Lett. **93**, 161909 (2008). https://doi.org/10.1063/1.3006320
34. S. Saito, T. Hosoi, H. Watanabe et al., First-principles study to obtain evidence of low interface defect density at Ge/ GeO_2 interfaces. Appl. Phys. Lett. **95**, 011908 (2009). https://doi.org/10.1063/1.3168501
35. J. Chastain, R.C. King Jr., *Handbook of X-ray photoelectron spectroscopy*, 1st edn. (Perkin-Elmer Corporation, Minnesota, 1979), p.88
36. N. Tabet, M. Faiz, N.M. Hamdan et al., High resolution XPS study of oxide layers grown on Ge substrates. Surf. Sci. **523**, 68–72 (2003). https://doi.org/10.1016/s0039-6028(02)02354-3
37. K. Kutsuki, G. Okamoto, T. Hosoi et al., Humidity-dependent stability of amorphous germanium nitrides fabricated by plasma nitridation. Appl. Phys. Lett. **91**, 163501 (2007). https://doi.org/10.1063/1.2799260
38. D.K. Schroder, *Semiconductor material and device characterization*, 1st edn. (Wiley, New york, 2005), pp.330–332
39. N. Novkovski, Refined analysis of C-V and I–V characteristics of Al/dielectric/Si structures containing nanosized Ta_2O_5/SiO_xN_y dielectric stack. J. Phys. D Appl. Phys. **54**, 055103 (2020). https://doi.org/10.1088/1361-6463/abbfc9
40. G. Dushaq, A. Nayfeh, M. Rasras, Passivation of Ge/high-κ interface using RF Plasma nitridation. Semicond. Sci. Technol. **33**, 015003 (2017). https://doi.org/10.1088/1361-6641/aa98cd
41. D.W. Yan, H. Lu, D.J. Chen et al., Distribution of deep-level traps at atomic-layer-deposited Al_2O_3/n-GaN interface. Solid State Electron. **72**, 56–59 (2012). https://doi.org/10.1016/j.sse.2012.02.012
42. Y.L. Yan, W.X. Zhong, S.T. Lin et al., Study on cosmogenic radioactive production in germanium as a background for future rare event search experiments. Nucl. Sci. Tech. **31**, 55 (2020). https://doi.org/10.1007/s41365-020-00762-1
43. R.M.J. Li, S.K. Liu, S.T. Lin et al., Identification of anomalous fast bulk events in a p-type point-contact germanium detector. Nucl. Sci. Tech. **33**, 57 (2022). https://doi.org/10.1007/s41365-022-01041-x